Traffic 2009; **10:** 1257–1271

doi: 10.1111/j.1600-0854.2009.00940.x

Exo70-Mediated Recruitment of Nucleoporin Nup62 at the Leading Edge of Migrating Cells is Required for Cell Migration

Thomas Hubert[1,2], Joël Vandekerckhove[1,2] and Jan Gettemans[1,2,*]

[1] *Department of Medical Protein Research, VIB, B-9000 Ghent, Belgium*
[2] *Department of Biochemistry, Ghent University, Faculty of Medicine and Health Sciences, Albert Baertsoenkaai 3, B-9000 Ghent, Belgium*
**Corresponding author: Jan Gettemans, jan.gettemans@ugent.be*

Nucleoporin Nup62 localizes at the central channel of the nuclear pore complex and is essential for nucleocytoplasmic transport. Through its FG-repeat domain, Nup62 regulates nuclear pore permeability and binds nuclear transport receptors. Here, we report that Nup62 interacts directly with Exo70 and colocalizes with Exo70 at the leading edge of migrating cells. Nup62 binds the N-terminal domain of Exo70 through its coiled-coil domain but not through its FG-repeat domain. Selective inhibition of leading edge Nup62 using RNA interference significantly reduces cell migration. Furthermore, Exo70 recruits Nup62 at the plasma membrane and at filopodia. Removal of the Exo70-binding domain of Nup62 prevents leading edge localization of Nup62. Analogous to Exo70, Nup62 cycles between the plasma membrane and the perinuclear recycling compartment. Altogether, we propose that Nup62 not solely regulates access to the cell nucleus, but additionally functions in conjunction with Exo70, a key regulator of exocytosis and actin dynamics, at the leading edge of migrating cells.

Key words: cell migration, Exo70, leading edge, nucleoporin, Nup62

Received 11 December 2008, revised and accepted for publication 4 May 2009, uncorrected manuscript published online 8 May 2009, published online 23 June 2009

Nucleoporins are the major components of the nuclear pore complex (NPC), a large proteinacious structure that perforates the nuclear envelope and controls nucleocytoplasmic transport of macromolecules (reviewed in (1)). Nucleoporin p62 (Nup62) is present in two NPC modules, the Nup62-Nup58-Nup45-Nup54 and the Nup214-Nup88-Nup62 subcomplexes (2). Nup62 is composed of two dissimilar domains: an intrinsically disordered FG-repeat containing N-terminal domain (amino acids 1–327) and an α-helical coiled-coil domain (amino acids 328–522). Nup62 is anchored at the NPC mainly via its coiled-coil domain that provides structure and targeting information (3–5). The FG-repeat domain on the other hand contributes directly to nucleocytoplasmic transport through direct interactions with nuclear transport receptors and – occasionally – with cargo (6,7). Nup62 interacts directly with nuclear transport factor 2 (NTF2) through its FG-repeat domain (8–10) and this interaction is essential for the transport activity of NTF2 (7,11). Systematic analysis of nucleoporin dynamics predicts both transport and structural roles for Nup62 at the NPC (12,13). Furthermore, intermolecular sliding between components of the Nup62-Nup58-Nup45-Nup54 complex in the central channel of the NPC is thought to regulate pore diameter (4).

Surprisingly, an increasing number of studies indicate that some nucleoporins also localize outside the NPC and are involved in a wide variety of processes apparently unrelated to NPC function, including microtubule regulation in the cytoplasm (14), mitochondria transport (15), gene transcription (16,17), DNA repair (18), centromere and kinetochore function in mitosis (19–21), spindle assembly (22,23) and metaphase to anaphase transition (24,25). Whereas some nucleoporins such as Nup358, Nup98 and the Nup84/Nup107 complex have been extensively linked to unexpected physiological functions, this has not yet been documented for Nup62.

Interestingly, nucleoporins also tend to perform additional functions at the NPC that are unrelated to nucleocytoplasmic transport. Examples are gene transcription at the yeast NPC (26), coupled nuclear import and sumoylation of the histone deacetylase HDAC4 by Nup358 (27) and targeting and repair of damaged DNA (18,28). Notably, some of these functions, such as Nup358-mediated sumoylation, are the same as those found at alternative subcellular localizations.

Exocyst component of 70kDa (Exo70) is a subunit of the exocyst complex, which is required for tethering of exocytotic vesicles at the plasma membrane. Delivery, tethering and fusion of exocytotic vesicles with the plasma membrane are essential for many cellular processes, including insulin secretion in pancreatic β-cells (29), targeting of matrix metalloproteinases (MMPs) to invadopodia in breast carcinoma cells (30), insulin-stimulated exocytosis of the glucose transporter Glut4 in 3T3L1 adipocytes (31), transport of low-density lipoprotein (LDL) receptors to the basolateral membrane of Madin-Darby canine kidney (MDCK) cells (32), granule secretion in platelets at sites of vascular injury (33), neurotransmitter release in the synapses of neurons (34), delivery of secretory vesicles to sites of dynamic plasma membrane expansion at

the leading edge of migrating cells (35) and membrane transport to the midbody ring of dividing HeLa cells to perform the physical separation of daughter cells (36).

The exocyst complex is evolutionarily conserved and is composed of eight subunits: Sec3, Sec5, Sec6, Sec8, Sec10, Sec15, Exo70 and Exo84. Exo70 interacts directly with phosphatidylinositol 4,5-bisphosphate (PIP_2) via its C-terminus, and together with Sec3 anchors the remaining exocyst subunits to the plasma membrane (37,38). Exo70 is composed of three domains (39): the N-domain (amino acids 1–393) that interacts with other exocyst subunits and with the small RhoGTPase TC10 (reviewed in (40)), and the C-terminus that interacts with the Arpc1A component of the Arp2/3 complex (41) and is composed of the M-domain (amino acids 394–538) and the C-domain (amino acids 539–653).

In many cell systems, expression of Exo70 induces multiple filopodia-like membrane protrusions. Exo70 has been shown to bind directly to the Arp2/3 complex in an EGF-regulated manner. Furthermore, inhibition of Exo70 represses Arp2/3 recruitment at the leading edge and blocks formation of actin-based membrane protrusions (41). Upon nerve growth factor (NGF)-induced differentiation of rat pheochromocytoma (PC12) cells, Exo70 interacts with the activated form of TC10 and targets the Exo70-TC10 complex to sites of membrane protrusions where it locally prevents Cdc42-dependent activation of Neural Wiskott-Aldrich syndrome protein (N-WASP), probably reflecting local morphological specialization (42).

Migration of eukaryotes requires coordinated adhesion, actin polymerization and sustained membrane traffic between the perinuclear recycling compartment and the leading edge of motile cells. Plasma membrane proteins such as integrins have been shown to be continuously internalized and recycled back to the cell front (reviewed in (43)). Delivery of transport vesicles at the cell surface involves vesicle tethering by the exocyst complex and SNARE-mediated fusion with the target membrane. Inhibition of vesicle delivery at the cell front impairs cell migration (44).

Generally, nucleoporins tend to display auxiliary functions in other cellular compartments or specialized structures such as the nuclear interior or the mitotic apparatus. It is therefore of interest to screen nucleoporins for unconventional localization and function. Moreover, nucleoporins with intrinsically disordered domains such as Nup62 are of special interest given that such domains have been found to be characteristic of higher organisms (45). In the present study, we report that Nup62 is required for cell migration and is recruited by Exo70 at the leading edge of migrating cells.

Results

Nup62 localizes at the leading edge of cells

Subcellular localization of Nup62 using immunofluorescence microscopy of cultured cells revealed that in addition to the expected nuclear membrane localization, Nup62 displays nucleoplasmic, perinuclear, cytoplasmic and midbody ring staining (Figure 1 and data not shown). Furthermore, HeLa cells that were stimulated with Epidermal growth factor (EGF) exhibited Nup62 recruitment at membrane protrusions resembling membrane ruffles (Figure 1A), and Human Embryonic Kidney 293 (HEK) cells transfected with the constitutively activated Rac Q61L mutant displayed Nup62 localization at induced lamellipodia (Figure 1B). In a sparsely seeded culture of Human prostate cancer (PC3) cells, Nup62 colocalized with Exo70 at lamellipodia (Figure 1C). To exclude a possible immunostaining artifact, we also analysed the subcellular localization of enhanced green fluorescent protein (EGFP)-coupled Nup62. Both EGFP-Nup62 and Nup62-EGFP localized at the nuclear membrane and

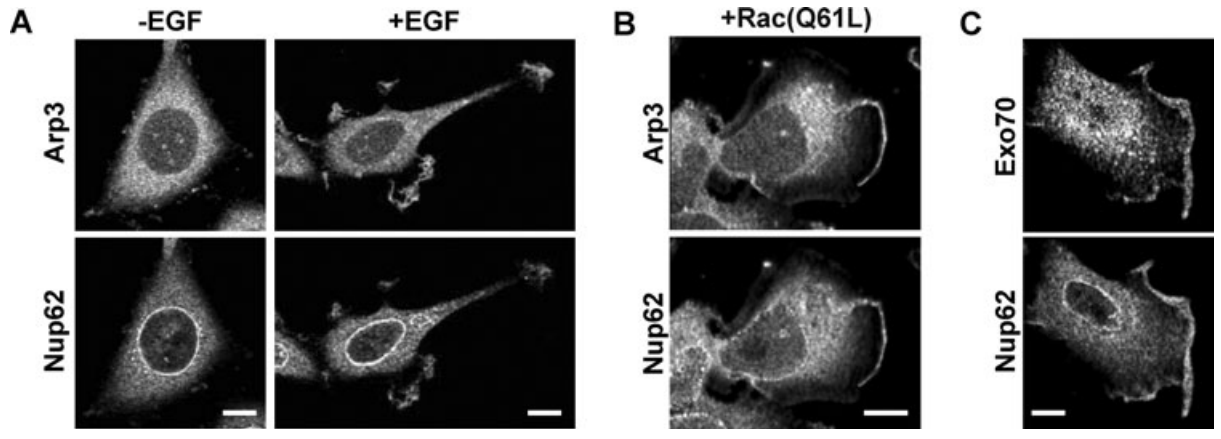

Figure 1: Nup62 localizes at the leading edge of migrating cells. A) Immunolocalization of endogenous Nup62 and Arp3 in EGF-stimulated HeLa cells and (B) in Rac Q61L transfected HEK cells. C) Colocalization of endogenous Nup62 and Exo70 at the cell leading edge in a sparsely seeded culture of PC3 cells. Scale bar, 10 μm.

at actin-related protein 3 (Arp3)-positive membrane protrusions (Figure S1A). Because nuclear pore Nup62 functions in the Nup62-Nup58-Nup45-Nup54 and Nup214-Nup88-Nup62 subcomplexes, we also investigated if we could detect these other nucleoporins at membrane protrusions. Nup88, Nup58/45 and Nup54 were found to localize at actin-based membrane protrusions (Figure S1B).

Colocalization with the midbody ring marker mitotic kinesin-like protein (MKLP1) in HeLa cells revealed that Nup62 localizes at the midbody ring just before or after completion of abscission (data not shown). Although it is known that the midbody ring persists for some time after abscission (36), no postmitotic function has yet been reported for the midbody ring.

Nup62 is involved in cell migration

As our results indicate that Nup62 is present at the leading edge of migrating cells, we postulated that Nup62 is involved in cell migration. To test this hypothesis, we down regulated Nup62 expression by RNA interference in PC3 cells and performed a standard wound-healing assay (Figure 2A). Nup62 down regulation was more than 90% (Figure 2B) and both cytoplasmic and leading edge Nup62 pools almost completely disappeared (Figure 2C). Mock-transfected cells and cells transfected with control small interfering RNAs behaved similarly and migrated about three times as far as cells transfected with Nup62 small interfering RNAs (1097 $\pm$ 125 μm and 1147 $\pm$ 40 μm versus 381 $\pm$ 194 μm and 386 $\pm$ 206 μm after 24 h). Thus, down regulation of cytoplasmic and leading edge Nup62 dramatically reduces cell migration. Immunofluorescence staining of cells from the wound-healing experiment revealed that the formation of membrane protrusions was not impaired as a consequence of Nup62 knock-down (Figure 2C). However, time lapse microscopy of PC3 cells transfected with Alexa 488-labelled siRNAs revealed that Nup62 knock-down cells developed larger ruffling lamellipodia and displayed reduced cell motility whereas cells transfected with control siRNAs migrated normally (supplementary video S1 and S2, Figure S2). This is consistent with a role for Nup62 in membrane transport to lamellipodia.

To exclude a possible effect of Nup62 knock-down on global nucleocytoplasmic transport events, we performed fluorescence-activated cell sorter (FACS) analysis on mock-transfected HeLa cells as well as on cells

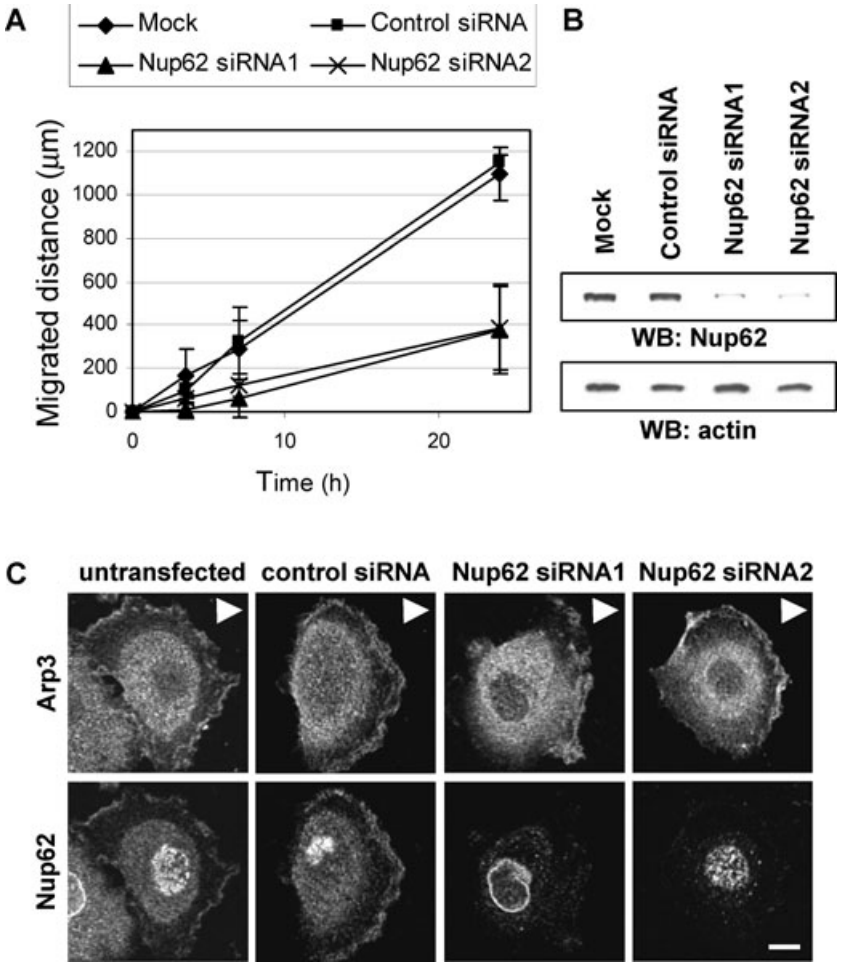

Figure 2: Nup62 regulates cell migration. A) Migrated distance over time of PC3 cells transfected with Nup62 siRNAs, control siRNA or without siRNA (mock) in a wound-healing assay. Nup62 knock-down reduces cell migration ($n = 9$). B) Nup62 knock-down was visualized by western blotting. Actin was added as a loading control. C) Immunolocalization of Nup62 and Arp3 at the cell leading edge in a wound-healing assay following Nup62 knock-down. Nup62 knock-down does not inhibit the formation of membrane protrusions. Note that untransfected cells were included instead of mock-transfected cells in (A). Arrowheads indicate the position of the wound. Scale bar, 10 μm.

transfected with either control siRNAs or Nup62 siRNAs. We reasoned that if nucleocytoplasmic transport is perturbed by Nup62 knock-down, this would have a major impact on cell cycle progression. However, Nup62 knock-down had no significant impact on cell cycle progression because the distribution of cells in the various cell cycle stages remained unaltered (Figure S3, left panels). We analysed transfection efficiency by immunofluorescence microscopy and noticed that almost all cells were transfected with the Nup62 siRNAs because they lacked cytoplasmic Nup62 staining in contrast to control cells (data not shown). This was further confirmed by the use of Alexa 488-labelled siRNAs that labelled virtually all cells (Figure S2). To attest that all cells enter the cell cycle normally, we arrested cells in M phase through nocodazole treatment to depolymerize microtubules. All cells entered mitosis normally after Nup62 knock-down because almost all cells have duplicated their DNA after 24 h (Figure S3, right panels).

Nup62 interacts directly with Exo70

To identify Nup62 interacting proteins, we selected five midbody ring proteins and analysed their interaction with Nup62 in a pull-down assay. Cep55, Annexin 11, Aurora B, Rab11 and Exo70 were expressed as streptavidin binding peptide (SBP)-fusion proteins in HEK cells together with untagged Nup62 and subsequently purified using streptavidin Sepharose. Of the tested proteins, only Exo70, a subunit of the exocyst complex, was able to bind to Nup62 (Figure 3A). The interaction between Nup62 and Exo70 was confirmed by co-immunoprecipitation experiments. NTF2 was used as a positive control for Nup62 binding (8) and Sec3, another exocyst subunit, was included to test the specificity of the interaction. EGFP-tagged Exo70, Sec3 or NTF2 were transfected in HEK cells together with untagged Nup62 and Nup62 was subsequently immunoprecipitated using anti-Nup62 antibody. Nup62 coprecipitated EGFP-Exo70, Exo70-EGFP and NTF2-EGFP but not EGFP-Sec3 and EGFP (Figure 3B, second panel from top). Reciprocally, using anti-EGFP antibody, EGFP-Exo70 and Exo70-EGFP but not EGFP-Sec3, EGFP and NTF2-EGFP coprecipitated Nup62 (Figure 3B, bottom panel). We also explored the *in vivo* interaction between both endogenous proteins. Therefore, we performed immunoprecipitations on PC3 cell extracts (Figure 3C). Anti-Exo70 antibody co-immunoprecipitated Sec8–another exocyst component – and Nup62 (Figure 3C, left panel). In contrast, anti-Sec8 antibody co-immunoprecipitated Exo70 but not Nup62 (Figure 3C, right panel). To determine if the proteins can also interact directly, we tested interaction between recombinant Exo70 and Nup62. Because all recombinant full-length Nup62 precipitates in inclusion bodies in *Escherichia coli* (3), we removed the intrinsically disordered FG-repeat containing domain and expressed only the coiled-coil domain (amino acids 328–522) fused to small ubiquitin-like modifier (SUMO) and V5 tags to improve solubility and detectability as the monoclonal anti-Nup62 antibody that we used only recognizes the N-terminal FG-repeat containing domain. After taking care that the tags are compatible and do not interfere in our experiment, we uncovered a direct binding between Exo70 and Nup62 (328–522) (Figure 3D).

Next, we examined the possibility that the direct interaction between Exo70 and Nup62 could reflect Nup62-assisted nuclear import of Exo70-EGFP. However, inhibition of Chromosome region maintenance 1 (CRM1)-mediated export of nuclear export sequence (NES)-containing proteins using Leptomycin B revealed no change in EGFP-Exo70 localization, suggesting that Exo70 is not shuttling between the cytoplasm and the nucleus (Figure S1C).

Exo70 recruits Nup62 at the plasma membrane and at filopodia

Exo70 recruits the Arp2/3 and exocyst complexes at sites of active membrane protrusion (41,46). Therefore, we wondered if Nup62 is also recruited at the plasma membrane by Exo70. When expressed in HEK cells, EGFP-Exo70 accumulated at the plasma membrane and induced numerous membrane protrusions (Figure 4A, right panel). Expressed untagged Nup62 on the other hand localized mainly in the cytoplasm at perinuclear vesicles and at membrane ruffles (Figure 4A, left panel). However, when Nup62 and Exo70 were expressed simultaneously, Nup62 relocalized to filopodia (Figure 4B, right panels), and an intense plasma membrane staining could be observed (Figure 4B, left panels). These findings indicate that Exo70, through interaction with Nup62, recruits the latter to filopodia and the plasma membrane.

Exo70 recruits Nup62 at internalized PIP_2-containing vesicles triggered by Arf6 Q67L or PIP5K

Exo70 and other exocyst subunits are continuously cycling between the perinuclear recycling compartment and the plasma membrane (47–49). Therefore, based on the previously described colocalization at the plasma membrane, we wondered if Nup62 could be recruited by Exo70 through the recycling pathway. EGFP-Exo70 normally localizes at the plasma membrane and at actin-based membrane protrusions ((41); Figure 5A, left panel). Exo70 associates with the plasma membrane through direct interaction between its C-terminus and PIP_2 (38,46). Furthermore, ADP-ribosylation factor 6 (Arf6) Q67L, a GTP hydrolysis-deficient mutant, and the Arf6 GTP downstream effector enzyme phosphatidylinositol-4-monophosphate 5-kinase (PIP5K) have been described to induce cytoplasmic accumulation and fusion of PIP_2-containing vesicles (50). These vesicles represent internalized membranes that are unable to recycle back to the plasma membrane because of a block in PIP_2 turnover and become trapped in the cytoplasm. When vesicles were induced in HEK cells by co-expression of Arf6 Q67L or PIP5K, we observed accumulation of internalized EGFP-Exo70 at the surface of these vesicles (Figure 5A, middle panel and 5C, right panel). A fusion protein of EGFP and the pleckstrin homology domain from PLCδ (EGFP-PH)

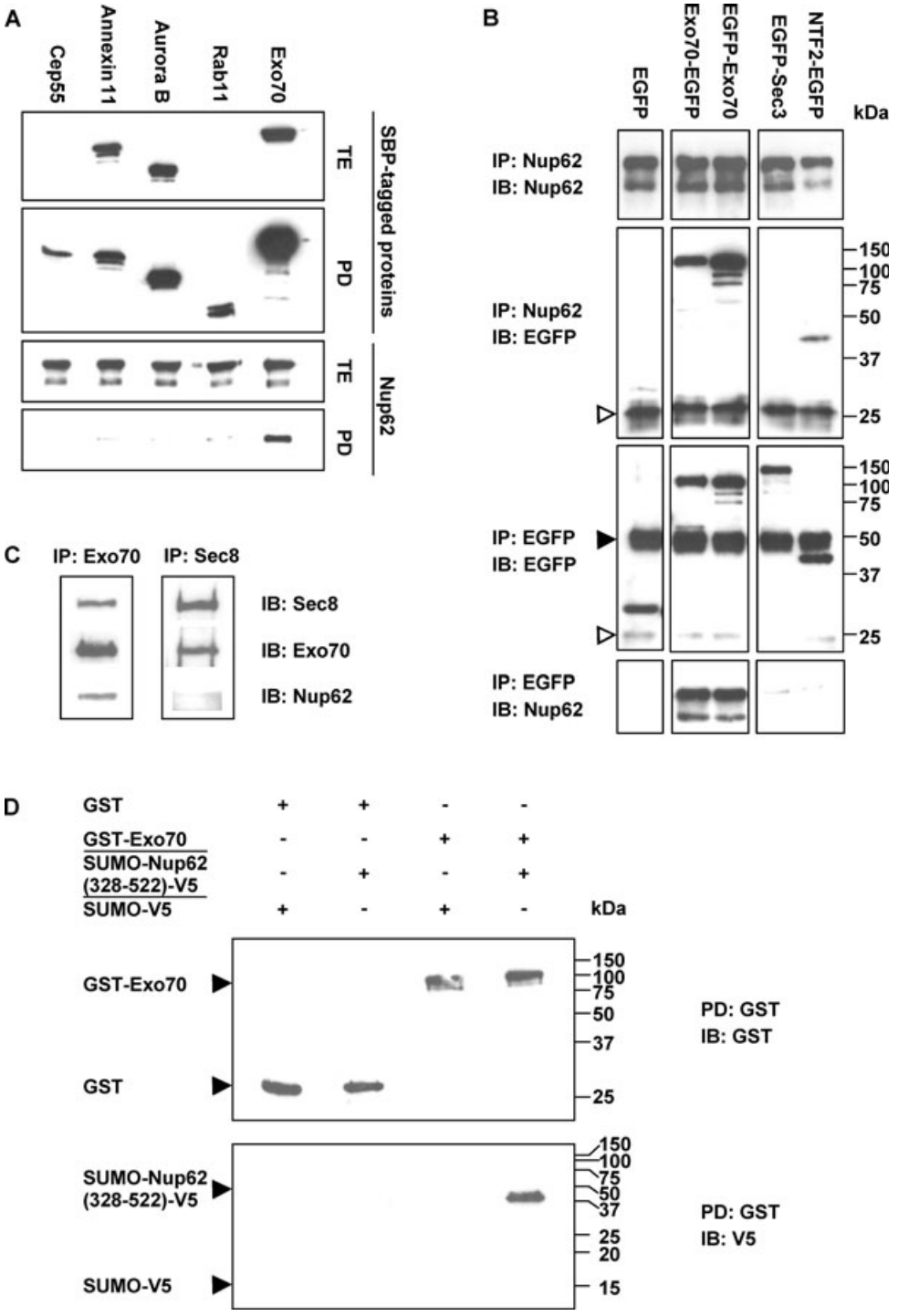

Figure 3: Nup62 interacts with Exo70. A) Pull-down (PD) of streptavidin binding peptide (SBP)-tagged proteins in HEK cell extracts using streptavidin Sepharose. The two upper panels show SBP-tagged proteins in total extracts (TE) and enriched on streptavidin Sepharose (PD). The lower panels show Nup62 in TE and pulled down by the SBP-tagged proteins. B) Immunoprecipitation (IP) of transfected HEK cell extracts using either anti-Nup62 mouse IgG (upper panels) or anti-EGFP rabbit IgG (lower panels). Proteins were detected by immunoblotting (IB). Open and full arrowheads are antibody light and heavy chains, respectively. C) Immunoprecipitation (IP) of endogenous proteins in PC3 cell extracts using either anti-Exo70 mouse IgG (left panel) or anti-Sec8 mouse IgG (right panel). Proteins were detected by IB. D) Recombinant GST and GST-Exo70 were incubated with equal amounts of recombinant SUMO-V5 or SUMO-Nup62(328–522)-V5 as indicated on top of the upper panel. GST PD was performed to determine if Nup62(328–522) can bind directly to Exo70. Precipitated GST constructs were identified by IB using anti-GST antibody. Coprecipitated SUMO-V5 constructs were identified by IB using anti-V5 antibody.

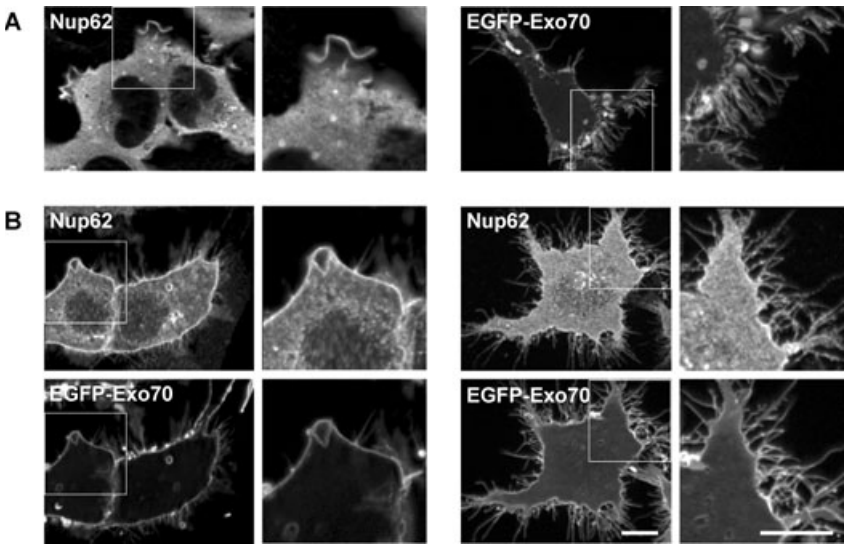

Figure 4: Exo70 recruits Nup62 at the plasma membrane and at filopodia. A) Untagged Nup62 and EGFP-Exo70 transfected separately in HEK cells. Note the localization of Nup62 in membrane ruffles and the formation of branched filopodia by Exo70. B) Nup62 and EGFP-Exo70 transfected simultaneously in HEK cells. Exo70 localization remains unaltered. Nup62, however, relocalizes to the plasma membrane (left pannels) and filopodia (right pannels) and colocalizes with Exo70. Scale bar, 10 μm.

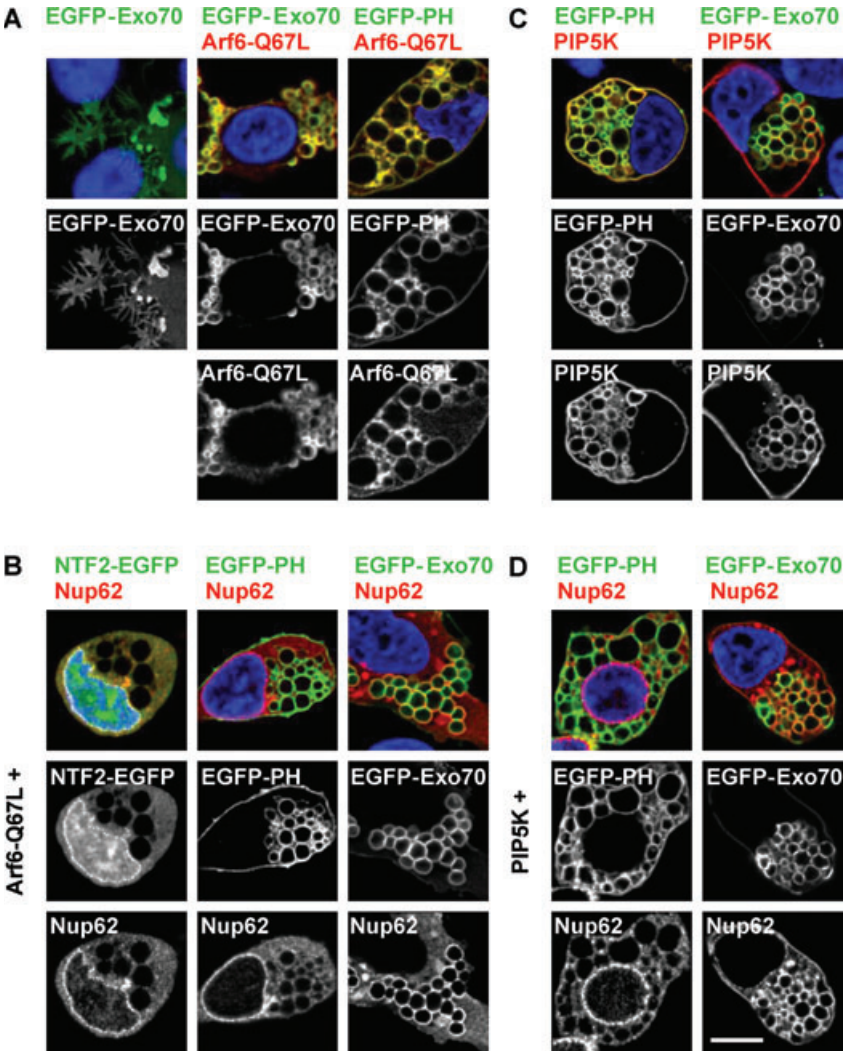

Figure 5: Exo70 recruits Nup62 on internalized membranes. Internalized plasma membrane was prohibited from recycling through expression of the constitutively activated Arf6-Q67L mutant (A, B) or the Arf6 effector PIP5 kinase (C, D). The PIP_2-enriched vesicles were coated with the PIP_2-binding proteins PH-PLCδ or with Exo70, as indicated. NTF2 binds to Nup62 but fails to localize at the vesicles and was included as a control (B). In the lower panels (B, D), untagged Nup62 was added as a third component. Nup62 is recruited by Exo70-coated vesicles but not by PH-PLCδ-coated vesicles (B, D). Scale bar, 10 μm.

visualizes PIP_2 accumulation at these vesicles (Figure 5A, right panel and 5C, left panel) and was further used as a negative control. Co-expressed untagged Nup62 was clearly targeted to the vesicles containing internalized EGFP-Exo70 (Figure 5B,D, right panels) but not to those containing internalized PH-EGFP (Figure 5B, middle panel and 5D, left panel), regardless if the vesicles were induced with Arf6 Q67L (Figure 5B) or PIP5K (Figure 5D). As expected, NTF2-EGFP which interacts with Nup62 but is not localized at the plasma membrane or the vesicles could not recruit Nup62 at the vesicles (Figure 5B, left panel).

Nup62 marks out the recycling pathway in conjunction with Exo70

We observed perinuclear localization of untagged Nup62 that concentrates in different parts around the centrosome (data not shown). Costaining with the Golgi marker cis-Golgi matrix protein of 130kDa (GM130) revealed no overlap (data not shown). However, expression of the constitutively inactive Ras-associated binding 11 (Rab11) S25N mutant showed almost complete overlap with the Nup62 staining pattern (Figure 6A), indicating that Nup62 localizes in a perinuclear compartment closely related to the recycling endosomes. Hypothetically, Nup62 is continually recycled between the perinuclear recycling compartment and the plasma membrane, similar to Exo70. To test this model, we blocked exocytic vesicle fusion with the plasma membrane using the GTPase-deficient TC10 Q75L mutant, a regulator of Exo70 (51). As expected, under these conditions EGFP-Exo70 accumulated in a dense membranous network in the cytoplasm (Figure 6B, left panel). The small size of the cells attests to the inhibition of membrane trafficking towards the plasma membrane. Interestingly, untagged Nup62 was recruited by Exo70 at these intracellular membranes (Figure 6B). These results implicate Nup62 in various stages of the recycling pathway, as evidenced by blocking distinct steps using GTPase constructs. Figure 6C schematically summarizes these findings.

Nup62 interacts with the N-domain of Exo70

To further characterize the binding with Exo70, we made Exo70-truncation constructs (shown in Figure 7A) and tested them on Nup62 binding in an immunoprecipitation assay (Figure 7B, results schematized in Figure 7A). All Exo70-truncation constructs containing the N-domain (full length, amino acids 1–538 and amino acids 1–393) bound to Nup62. In contrast, all constructs lacking the N-domain failed to bind Nup62 (amino acids 539–653 and amino acids 394–653). To confirm these results, we used the Exo70-truncation constructs in Arf6 Q67L transfected HEK cells to determine the *in vivo* effect on Nup62 localization (Figure 7C). The Exo70 N-domain that interacts with Nup62, but does not contain the membrane targeting domain, failed to internalize with plasma membrane and consequently did not coat the surface of vesicles (Figure 7C, middle panel). Accordingly, Nup62 was not recruited to these vesicles (Figure 7C, middle panel). The

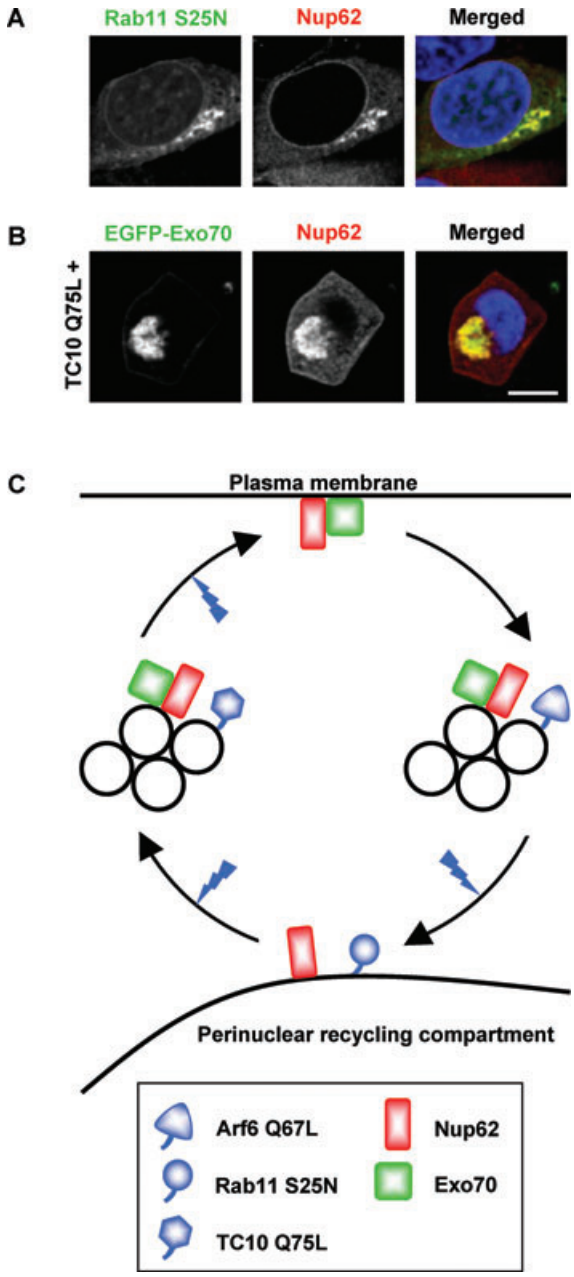

Figure 6: Nup62 localizes at the perinuclear recycling compartment and is recruited by Exo70 at exocytic vesicles. A) Colocalization of Nup62 and the constitutively inactivated Rab11 S25N mutant in the perinuclear recycling compartment. B) Membrane trafficking to the plasma membrane was blocked by the constitutively activated TC10 Q75L mutant, preventing vesicle fusion with the plasma membrane and resulting in accumulation of exocytic vesicles in the cytoplasm. Addition of Exo70 and Nup62 results in recruitment of Nup62 at Exo70 containing exocytic vesicles. C) Schematic overview of the data presented in Figures 4, 5 and 6. Exocyst regulating GTPases Arf6, Rab11 and TC10 were used to demonstrate the linkage between Exo70 and Nup62 through the recycling pathway. Blue arrows indicate disrupted processes by corresponding GTPase mutants. Scale bar, 10 μm.

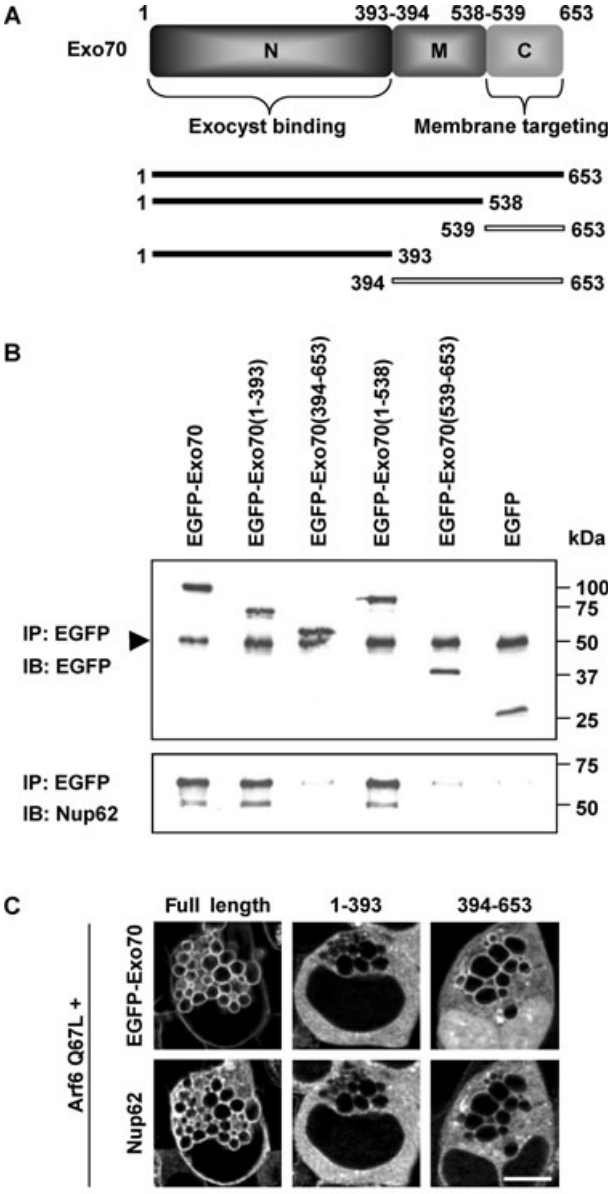

Figure 7: Nup62 interacts with the N-domain of Exo70. The N-domain of Exo70 is required for interaction with Nup62 inside living cells. A) Schematic representation of the Exo70 domains. Positions of first and last amino acids of the domains are indicated. Exo70 fragments that were used in the immunoprecipitation assay are represented by bars. Full bars indicate interaction with Nup62. Open bars indicate no interaction with Nup62. B) Immunoprecipitation (IP) of double-transfected HEK cell extracts using anti-EGFP rabbit IgG. Immunoprecipitated EGFP-tagged full-length, N-domain (amino acids 1–393), M- and C-domain (amino acids 394–653), N- and M-domain (amino acids 1–538) and C-domain (amino acids 539–653) of Exo70 were visualized by immunoblotting (IB) in the upper panel. Co-immunoprecipitated Nup62 was visualized in the lower panel. Full arrowhead indicates antibody heavy chain. C) Internalized plasma membrane arrested in vesicles as a result of transfection with the constitutively activated Arf6-Q67L mutant. Full-length Exo70 and the M- and C-domain (amino acids 394–653) of Exo70 contain the membrane targeting domain and are internalized (left and right upper panels). The N-domain (amino acids 1–393) of Exo70 does not contain the membrane targeting domain and is not internalized (middle upper panel). Nup62 internalization is visualized in the lower panels. Scale bar, 10 μm.

complementary Exo70 fragment containing the M- and the C-domains was enriched at the vesicles but did not recruit Nup62, in line with the results of the immunoprecipitation assay. Although implicit, this information points towards an essential role for the Exo70 N-domain in Nup62–Exo70 interaction *in vivo*.

Exo70 binds to the coiled-coil domain of Nup62

Nup62 contains an intrinsically unstructured FG-repeat containing N-terminal domain (amino acids 1–325) that supports nucleocytoplasmic exchange of macromolecules by means of direct contacts with nuclear transport receptors, and a C-terminal coiled-coil domain (amino acids 328–522) that contributes to anchoring Nup62 at the NPC. To determine the Exo70 binding site in Nup62, we tested these Nup62 domains separately in an immunoprecipitation assay (Figure 8B, results schematized in Figure 8A). EGFP-Exo70 bound to full-length Nup62 and to the coiled-coil domain of Nup62 but not to the FG-repeat domain of Nup62 (Figure 8B, first three lanes). The N-domain of Exo70 also bound to full-length Nup62 and the coiled-coil domain of Nup62 (Figure 8B, last two lanes). To confirm these results *in vivo*, we took advantage of the ability of Exo70 to recruit Nup62 at filopodia and the plasma membrane. When co-expressed, Exo70 recruited the coiled-coil domain

Figure 8: Exo70 interacts with the coiled-coil domain but not with the FG-repeat domain of Nup62. A) Schematic representation of the Nup62 domains. Positions of first and last amino acids of the domains are indicated. Nup62 fragments that were used in the immunoprecipitation assay are represented by bars. Full bars indicate interaction with Exo70. Open bars indicate no interaction with Exo70. B) Immunoprecipitation (IP) of double-transfected HEK cell extracts using anti-EGFP rabbit IgG. The Nup62 fragments are referred to as A (full length), B (amino acids 1–325) and C (amino acids 328–522) according to the schematic representation above. The upper panel shows V5-tagged Nup62 fragments in total extracts (TE). The lower panel shows immunoprecipitated EGFP-Exo70 (first three lanes) and EGFP-Exo70N (N-domain, amino acids 1–393 of Exo70; last two lanes). The central panel shows co-immunoprecipitated Nup62 fragments. C) FG-repeat fragment of Nup62 (amino acids 1–325) localizes at multiple vesicle-like structures near actin-based membrane protrusions in HEK cells. Actin filaments were visualized by phalloidin staining. D) Co-expression of EGFP-Exo70 and the FG-repeat fragment of Nup62. The FG-repeat fragment is not targeted to the plasma membrane (left panels) or filopodia (right panels). E) Co-expression of EGFP-Exo70 and the coiled-coil fragment of Nup62. The coiled-coil fragment is targeted to the plasma membrane (left panels) and filopodia (right panels). Scale bars, 10 μm.

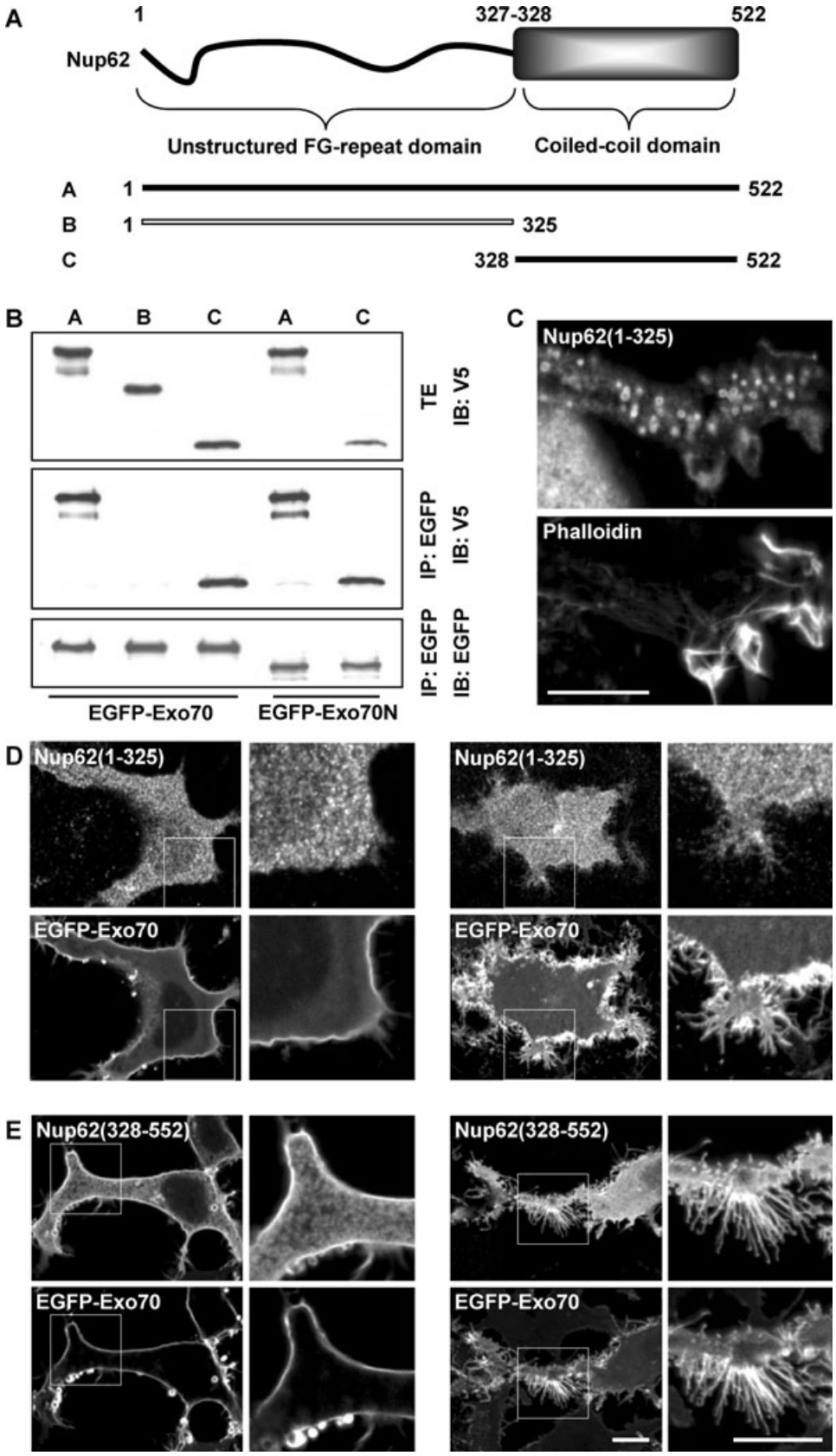

Figure 8: Legend on previous page.

of Nup62 to both filopodia (Figure 8E, right panels) and the plasma membrane (Figure 8E, left panels) with equivalent intensity as full-length Nup62 (Figure 4). On the contrary, the FG-repeat domain of Nup62 remained entirely insensitive to Exo70 and was not recruited to the plasma membrane (Figure 8D, left panels) and filopodia (Figure 8D, right panels). Altogether, these results indicate that the N-domain of Exo70 interacts with the coiled-coil domain of Nup62 but not with the FG-repeat domain. Interestingly, the FG-repeat domain of Nup62 localized at a multitude of vesicles that specifically concentrated near actin-based membrane protrusions (Figure 8C).

Removal of the Exo70-binding domain of Nup62 prevents leading edge localization of Nup62

Expression of the coiled-coil domain of Nup62 revealed a large increase in the perinuclear localization of Nup62, indicating that the cycling of Nup62 was impaired, resulting in an accumulation of the Nup62 fragment in the perinuclear recycling compartment (Figure 9B, upper left panels; results schematized in Figure 9A). These results indicate that the FG-repeat domain of Nup62 is needed for transport of Nup62 from the perinuclear recycling compartment to the plasma membrane. Expression of the FG-repeat domain of Nup62 showed two interesting localization motifs. First, this domain decorated microtubules but not actin filaments (Figure 9B, upper right panels and data not shown; results schematized in Figure 9A), suggesting a possible transient association of Nup62 with microtubules via a motor protein. This characteristic explains how Nup62 might be transported to the cell surface and why deletion of this domain results in retention of Nup62 in the perinuclear recycling compartment. Accordingly, when microtubules are depolymerized by nocodazole treatment, the localization of the FG-repeat domain of Nup62 becomes completely uniform throughout the cell, lacking any subcellular accumulation (Figure S1D). Second, the FG-repeat domain of Nup62 accumulated in densely packed vesicle-like structures in the vicinity of membrane protrusions (Figures 8C and 9B, lower panels; results schematized in Figure 9A). This pool is prevented from associating with the plasma membrane because of the absence of the coiled-coil domain. Thus, equivalently, removal of the Exo70-binding domain results in impaired docking at membrane protrusions.

Discussion

Nucleoporins constitute the pores in the nuclear membrane through which all nucleocytoplasmic transport occurs (reviewed in (52)). Most proteins that need to cross the nuclear membrane require nuclear transport receptors that depend on nucleoporins for translocation. Nup62 is a nucleoporin that localizes in the central channel of the NPC (53) and occasionally also binds cargo directly to support nuclear import (7). So far, Nup62 has never been reported in other compartments of the cell. Therefore, the most obvious explanation for the Nup62–Exo70 interaction described here would be Nup62-assisted nuclear import of Exo70. However, both endogenous Exo70 staining using a monoclonal antibody (41) and expression of EGFP-tagged Exo70 (46) revealed no sign of nuclear localization of Exo70. Moreover, none of our Exo70 truncation constructs localized in the nucleus except those with a molecular mass below the limit for passive diffusion which is estimated at 30–60 kDa (Figure 7C and data not shown). Nevertheless, the rabbit anti-Exo70 antibody used in this study gives some uniform nuclear staining. As a result, we cannot exclude completely the possibility that Nup62 assists Exo70 in nuclear transport. Even so, the presence of Nup62 at the leading edge and the recruitment of Nup62 at the plasma membrane and filopodia by Exo70 indicate an alternative function for the Nup62–Exo70 interaction. Moreover, Exo70 interacts with the coiled-coil domain of Nup62 and not with the FG-repeat domain that supports nucleocytoplasmic transport (7,52).

In this study, we report a major pool of Nup62 in the cytoplasm. High levels of cytoplasmic Nup88 have also been observed by others but this has not been further studied so far (54). RNA interference of Nup62 with two independent siRNA duplexes greatly reduced the cytoplasmic pool of Nup62 without affecting the NPC pool. Furthermore, Nup62 is no longer recruited to the leading edge after Nup62 RNA interference. This indicates that the cytoplamic and leading edge Nup62 stainings are not staining artefacts but represent important Nup62 pools that have not been investigated so far. The sustained localization of Nup62 at the nuclear membrane up to 72 h after siRNA transfection is surprising as the overall residence time of Nup62 at the NPC has been estimated at 13 h, which is significantly less than that of structural scaffold nucleoporins (12). This probably reflects incomplete Nup62 mRNA degradation and preferential replenishment

Figure 9: Expression of Nup62 fragments. A) Schematic representation of the subcellular localization of Nup62 and Nup62 fragments shown in (B). N, nucleus. B) Expression of Nup62 and Nup62 fragments in HEK cells. Full-length Nup62 (amino acids 1–522) localizes at membrane protrusions and at the perinuclear recycling compartment. The coiled-coil domain of Nup62 (amino acids 328–522) accumulates strongly in the perinuclear recycling compartment. The FG-repeat fragment of Nup62 (amino acids 1–325) localizes at microtubules (α-tubulin; upper right panels) and concentrates at vesicle-like structures in the neighbourhood of membrane protrusions (lower panels). Blue, DAPI. Scale bars, 10 μm. C) Model of Nup62 and Exo70 functioning. Question marks indicate unknown microtubule motor protein complex and unknown effect on exocytosis. Blue arrows indicate disrupted processes by corresponding Nup62 domain deletions. Deletion of the FG-repeat domain results in a block of Nup62 transport and, consequently, a strong accumulation of Nup62 at the perinuclear recycling compartment. Removal of the Exo70-binding domain of Nup62 prevents plasma membrane localization of Nup62. MT, microtubule; PNRC, perinuclear recycling compartment.

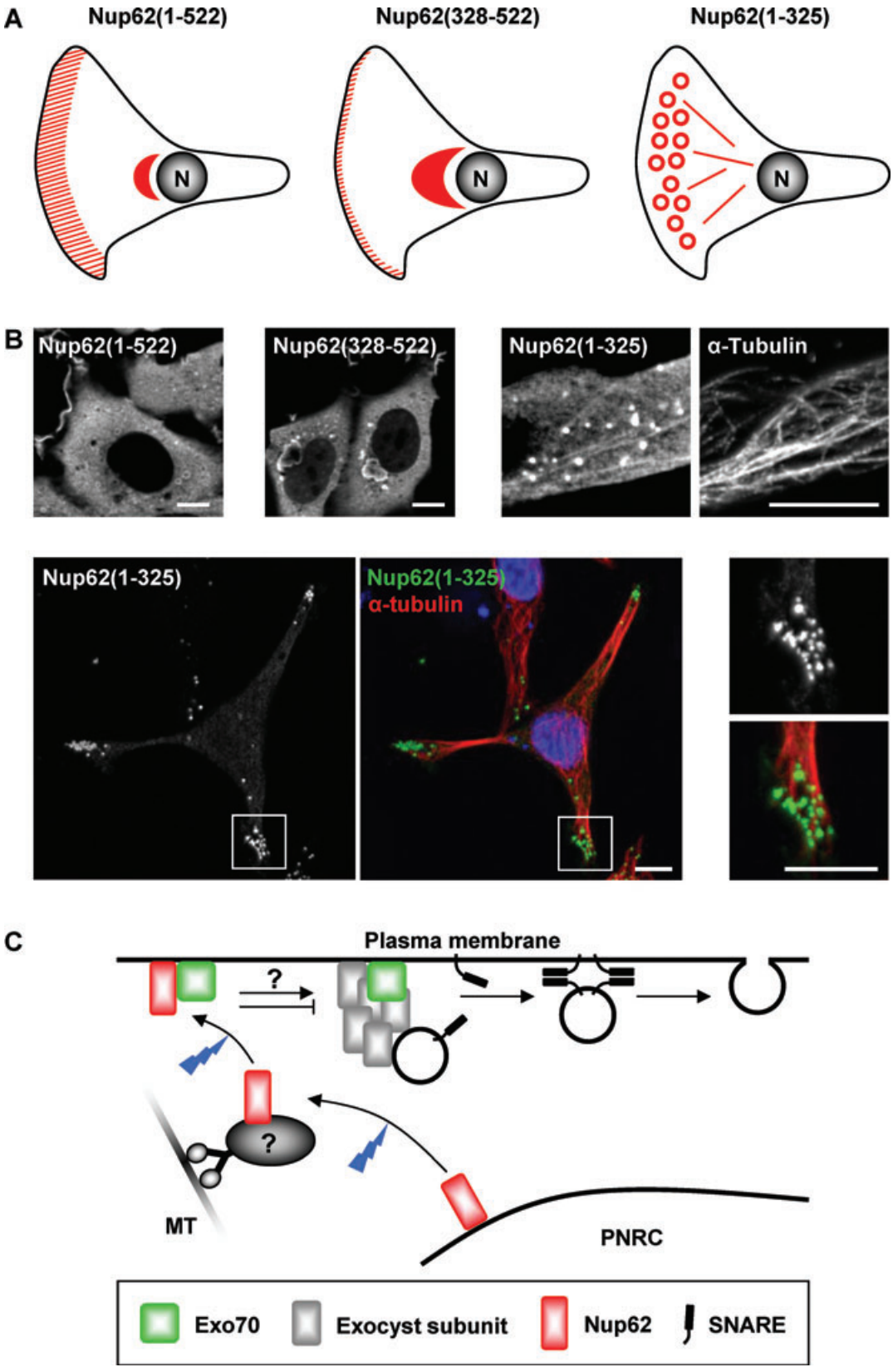

Figure 9: Legend on previous page.

of the essential Nup62 pool at the NPC. Alternatively, the residual amount of Nup62 seen in the western blot and immunostaining could represent a stable subpopulation due to protective complex formation or post-translational modification. Whatever the cause, this partial knock-down allowed us to study specifically the function of cytoplasmic and leading edge Nup62 without having to deal with perturbation of nucleocytoplasmic transport which would have a major impact on cell homeostasis.

At the leading edge, Exo70 is known to be indispensable for two aspects of cell migration: recruitment of the actin polymerization factor Arp2/3 (41) and targeting of exocytic vesicles (38). In migrating PC3 cells, in Rac Q61L transfected HEK cells or in EGF-stimulated HeLa cells, Nup62 is targeted to the leading edge. Relocalization of Nup62 to the leading edge was completely inhibited after Nup62 RNA interference. Simultaneous expression of Nup62 and Exo70 revealed that Nup62 is recruited by Exo70. Exo70 knock-down would therefore be expected to block Nup62 relocalization to the cells front. This prediction however cannot be verified because inhibition of Exo70 prevents formation of actin-based membrane protrusions (41). To circumvent this problem, we removed the Exo70-binding domain of Nup62, resulting in impaired leading edge localization of Nup62. Inversely, Nup62 knock-down did not block Arp3 localization at membrane protrusions and thus does not interfere with the ability of Exo70 to recruit the Arp2/3 complex (41). Nevertheless, Nup62 has an active role in cell migration as reflected by the dramatic reduction in migrated distance of cells lacking Nup62 in the cytoplasm and at the leading edge.

Exo70 and other exocyst components also localize to other cellular compartments, including the Golgi apparatus, the *trans* Golgi network, the early endosomes and Rab11-positive recycling endosomes (49). Exo70 is likely to continuously cycle between these compartments and the plasma membrane. Based on the observation that expressed untagged Nup62 localizes at a pericentriolar organelle (data not shown), we considered possible recycling of Nup62. We first identified this organelle as related to the Rab11-positive recycling endosomes. To study other steps in the recycling pathway, we blocked trafficking membrane from and towards the plasma membrane using constitutively activated Arf6 and TC10 (two exocyst-regulating small GTPases), respectively (50,51). In both cases, as trafficking membranes became trapped in large cytoplasmic pools, Exo70 was able to recruit Nup62 at the surface of these membranes. These results suggest that Nup62 is able to accompany Exo70 through the recycling pathway. Furthermore, when the recycling of Nup62 is blocked by deleting its FG-repeat domain, Nup62 strongly accumulates in the perinuclear recycling compartment.

Exo70 interacts via its N-terminal domain with the coiled-coil domain of Nup62. The delineation of the interaction interface raises two important questions. First, since it is through its N-terminal domain that Exo70 recruits the other exocyst subunits, Nup62 may possibly facilitate, compete for, or sense complex formation and thus influence exocyst complex formation directly or indirectly. However, it should be noted that sec3 and sec8—two other exocyst components – failed to interact with Nup62. Second, as suggested in Figure 8C, the FG-repeat domain of Nup62 may well be involved in exocytosis but does not bind Exo70. Indeed, without structural and targeting information provided by the coiled-coil domain, Nup62 localizes at numerous vesicles near membrane protrusions. Possibly, Nup62 binds other components of the membrane trafficking pathway through its FG-repeat domain. One such candidate is Syntaxin 2, a SNARE protein involved in membrane fusion. Preliminary findings point to an interaction between Nup62 and Syntaxin 2 (data not shown) but these data have to be interpreted carefully because both the FG-repeat domain of Nup62 and SNARE proteins contain hydrophobic domains.

Because nucleoporins tend to function in stable multicomponent modules both in interphase and in mitosis (2,55), Nup62 most likely cooperates with other components of the Nup62-Nup58-Nup45-Nup54 and Nup214-Nup88-Nup62 subcomplexes at the cells front. It is puzzling that both structural scaffold (Nup84/Nup107 complex), structural adaptor (Nup98 and Nup62 complexes) and dynamic (Nup153) nucleoporin modules have been assigned alternate cellular tasks (12). Furthermore, these nucleoporin modules tend to regulate highly dynamic and complex molecular machines such as the NPC, the anaphase promoting complex (APC), the kinetochore, the mitotic spindle and possibly the transcriptosome (56). This study adds the exocyst complex as a possible target of a nucleoporin module.

Nevertheless, non-canonical nucleoporin functions appear more comprehensible in the context of recent insights into normal interphase NPC functioning. For example, Nup358 is a nucleoporin with SUMO E3 ligase activity that stably interacts with the SUMO E2-conjugating enzyme Ubc9 at the NPC (57). Surprisingly, in mitosis, topoisomerase IIα requires sumoylation by Nup358 to localize correctly at the centromeres to decatenate sister centromeres before anaphase (21). This unexpected function of Nup358 in mitosis is quite remarkable but is certainly made more comprehensible by the finding that, in interphase, Nup358 also sumoylates HDAC4 deacetylase at the entrance of the nuclear pore (27). In addition, other (de)sumoylation enzymes necessitate NPC localization to work properly (18). Thus, the view emerges that the cell exploits the central position of the nuclear pore to perform additional tasks at the NPC such as (de)sumoylation (58). This may explain why numerous nucleoporins have extended their work field beyond the nuclear pore, which makes little sense from the viewpoint of nucleocytoplasmic transport alone (56). In this perspective, exploring the functioning of Nup62 at the cell front might also lead to new insights into the working of the NPC.

Materials and Methods

Plasmids and siRNAs

Nup62 (IRATp970E1077D), Cep55 (IRAUp969A0230D), Annexin 11 (IRAUp969G0537D) and Aurora B (IRAUp969D1049D) were obtained from ImaGenes (Germany). EGFP-rab11 and EGFP-rab11 S25N were a kind gift from Professor S. Ferguson (Robarts Research Institute London, ON, Canada). Myc-TC10 Q75L plasmid was a kind gift from Professor J. Pessin (Albert Einstein College of Medicine, NY, USA). The NTF2 cDNA was a kind gift from Professor J. P. Siebrasse (Institut für Medizinische Physik und Biophysik, Universität Münster, Germany). EGFP-Sec3, Exo70-EGFP and EGFP-Exo70 plamids were a kind gift from Dr R. Scheller (Genentech Inc.). HA-Arf6-Q67L was a kind gift from Dr B. Wehrle-Haller (Centre Medical Universitaire, Geneva, Switzerland). Myc-tagged PIP5 kinase 1α was previously used (59). EGFP-PH-PLCδ was previously described (60). GST-Exo70 was a kind gift from Dr W. Guo (University of Pennsylvania, PA, USA). cDNAs were subcloned into the EGFP-N1 vector, the EGFP-C1 vector (Clontech-Takara Bio Europe) or the pCTAP-A vector containing the SBP and calmodulin binding peptide (CBP) sequences (InterPlay™ Mammalian TAP System; Stratagene). V5 tag (GKPIPNPLLGLDST) was cloned in the pET SUMO vector (Invitrogen). pGEX−5X−1 vector was from GE Healthcare. Nup62 fragments were subcloned into the pcDNA3.1/V5-His/TOPO or the pET SUMO vector (Invitrogen). Small interfering RNAs against Nup62 were purchased from Eurogentec (Nup62 siRNA1 = CCUACAAGCUGGCUGAGAAtt + UUCUCAGCCAGCUUGUAGGtt; Nup62 siRNA2 = GCAACUGCUCCAACCUCAUtt + AUGAGGUUGGAGCAGUUGCtt).

Antibodies

The following antibodies were used: mouse antibody to Nup62, clone 53 (BD Biosciences Pharmingen #610497); mouse antibody to CBP tag (Upstate #07–482); rat anti-HA antibody, clone 3F10 (Roche #1867423); mouse antibody to actin, clone C4 (MP Biomedicals #691001); mouse antibody to V5 (Invitrogen #R960−25); mouse antibody to Exo70 (Abcam #ab57402); mouse antibody to Sec8 (BD Transduction Laboratories #610658), goat antibody to glutathione S-transferase (GST) (GE Healthcare #27457701). Mouse antibody to myc and rabbit antibody to EGFP were home made. Rabbit Exo70 antibody was a kind gift from Professor C. Yeaman (University of Iowa, USA). Secondary antibodies and Alexa Fluor 488-tagged phalloidine were from Molecular Probes (Invitrogen).

Cell culture and transfection

PC3 cells were maintained at 37°C in a humidified 10% CO_2 incubator and grown in RPMI−1640 (Gibco BRL Life Technologies) supplemented with 10% fetal bovine serum, 100 μg/mL streptomycin and 100 IU/mL penicillin. HeLa and HEK293T cells were grown in DMEM with 10% fetal bovine serum, 100 μg/mL streptomycin and 100 IU/mL penicillin. HeLa and PC3 cells were transiently transfected using lipofectamine reagent (Invitrogen) according to the manufacturer's instructions. HEK293T cells, seeded on rat tail collagen-coated coverslips, were transfected using calcium phosphate. For EGF (Sigma-Aldrich) treatment, HeLa cells were plated on collagen-coated coverslips, serum starved overnight and subsequently stimulated with 20 ng/mL EGF for 3 up to 15 min before processing for immunofluorescence microscopy.

Pull-down, immunoprecipitation, in vitro binding and western blotting

Cells were disrupted in ice-cold lysis buffer [50 mM Tris–HCl pH 7.5, 150 mM NaCl, 1 mM MgAc, 1% Triton-X−100, 2 mM dithiothreitol, 5 mM sodium fluoride, 2 mM sodium orthovanadate, 1 mM phenylmethylsulphonyl fluoride (PMSF) and a protease inhibitor cocktail mix] using a tip sonicator. Insoluble material was removed by centrifugation (14000× ***g*** for 10 min at 4°C). Protein concentrations were determined by the method of Bradford (61) using BSA as a standard. For immunoprecipitation, 500 μg of cleared cell lysate was incubated with 1 μg antibody for 2 h at 4°C and bound proteins were recovered with protein G–Sepharose (GE Healthcare). For pull-downs, 500 μg of cell lysate was incubated with 40 μL of streptavidin resin slurry (Pierce) for 2 h at 4°C. For *in vitro* binding of GST/GST-Exo70 with SUMO-V5/SUMO-Nup62(328–522)-V5, proteins were expressed in TOP10 or BL21(DE3) (Invitrogen) cells, respectively, after induction with 1 mM IPTG, overnight at 20°C. Equal amounts of cell extracts were incubated, washed and purified using Glutathion Sepharose 4 Fast Flow (GE Healthcare Bio-Sciences). Western blotting was performed as described (62). Proteins were visualized by enhanced chemiluminescence detection (Amersham Pharmacia Biotech).

Immunostaining and immunofluorescence microscopy

For fixation, cells were washed with PBS, fixed with 3% paraformaldehyde for 20 min at room temperature and permeabilized with 0.2% Triton-X−100 in PBS for 5 min. Paraformaldehyde was neutralized with 0.75% glycine for 20 min. Cells were then blocked in 1% BSA in PBS for 30 min and incubated with primary antibody for 1 h at 37°C. Cells were washed in PBS, then incubated with secondary antibody (Alexa 488-conjugated goat anti-rabbit or Alexa 594-conjugated goat anti-mouse; Molecular Probes) and 4,6-diamidino−2-phenylindole (DAPI; Sigma) for 30 min at room temperature. Following immunostaining, samples were analysed using a Carl Zeiss Axiovert 200M Apotome epifluorescence microscope [63x 1.4 numerical aperture (NA) oil objective] equipped with an Axiocam cooled charge-coupled device (CCD) camera and processed using Axiovision software (Zeiss).

Wound-healing assay

PC3 cells ($n = 900000$) were seeded into six-well cell culture plates. Twenty-four hours after seeding, cells were transfected with either Nup62 siRNA1, with Nup62 siRNA2, with the negative control siRNA provided by Eurogentec or with water (mock). Forty-eight hours after transfection wounds were made by scratching three lines in a confluent monolayer. For each line, three measure points were marked resulting in nine measure points per well. Cell debris was removed by extensively washing the cells with PBS and medium. After 0, 4, 8 and 24 h the width of the wound was measured at the marked locations.

Acknowledgments

The authors are grateful to Dr Charles Yeaman for kindly providing a rabbit Exo70 antibody and to Dr L. Gerace for the Nup58/45 and Nup54 antibodies. We also wish to thank Dr Richard Scheller for the EGFP-Sec3 and EGFP-Exo70 plasmids, Dr S. Ferguson for the EGFP-rab11 constructs, Dr J. P. Siebrasse for the NTF2 cDNA, Dr J. Pessin for the TC10 construct and Dr W. Guo for the GST-Exo70 plasmid. We thank Dr V. De Corte for the EGFP antibody, Dr A. De Ganck for the myc antibody, Dr K. Meerschaert for helpful discussion and Dr A. Lambrechts for the Arp3 antibody and time lapse microscopy. This work was supported by the Concerted Actions Program of Ghent University (GOA), the IUAP programme, the human Frontier Science Program (HFSP), the Fund for Scientific Research-Flanders (FWO-Vlaanderen) and the Vlaamse liga tegen kanker.

Supporting Information

Additional Supporting Information may be found in the online version of this article:

Figure S1: Immunofluorescence microscopy experiments. A) HEK cells were transfected with EGFP-Nup62 or Nup62-EGFP and subsequently stained for Arp3 to demonstrate the presence of EGFP-tagged Nup62 in membrane protrusions (enlarged areas). B) HEK cells were stained for Nup88, Nup58/45, Nup54 and Arp3 or Nup62 to demonstrate the presence of Nup88, Nup58/45 and Nup54 in membrane protrusions (enlarged areas).

C) EGFP-Exo70 in control and Leptomycin B (LMB)-treated HEK cells. D) HEK cells were transfected with Nup62(1–325)-V5 and subsequently treated with nocodazole to depolymerize microtubules. α-Tubulin staining shows depolymerized microtubules. V5 staining shows the localization of Nup62(1–325)-V5. Scale bar, 10 μm.

Figure S2: Time lapse microscopy of Nup62 knock-down cells. PC3 cells were transfected with Alexa 488-conjugated control siRNAs or Nup62 siRNAs and stained for Nup62 to demonstrate the efficacy of the knock-down.

Figure S3: Nup62 knock-down does not interfere with cell cycle entry or cell cycle distribution in a HeLa cell population. FACS analysis of HeLa cells transfected with water (mock), control siRNAs of Nup62 siRNAs, as indicated at the left. The purple diagrams represent the distribution of cells in function of their DNA content as measured by propidium iodide (PI) fluorescence (left panels). The first maximum in the distribution corresponds to 2n or G1 cells, while the second, lower, maximum corresponds to 4n or M cells. In between the two maxima are the replicating cells with a DNA content between 2n and 4n. To analyse cell cycle entry, cells were treated with nocodazole to depolymerize microtubules and arrest cells in M phase (right panels). As a result, cells are blocked when they have a 4n DNA content and the higher maximum in the diagram shifts from 2n to 4n.

Video S1: Control cells migrate normally. Time lapse video of 30 min of PC3 cells transfected with control siRNA.

Video S2: Nup62 knock-down cells show disrupted cell migration. Time lapse video of 30 min of PC3 cells transfected with Nup62 siRNA1.

Please note: Wiley-Blackwell are not responsible for the content or functionality of any supporting materials supplied by the authors. Any queries (other than missing material) should be directed to the corresponding author for the article.

References

1. Terry LJ, Shows EB, Wente SR. Crossing the nuclear envelope: hierarchical regulation of nucleocytoplasmic transport. Science 2007;318:1412–1416.
2. Macaulay C, Meier E, Forbes DJ. Differential mitotic phosphorylation of proteins of the nuclear pore complex. J Biol Chem 1995;270:254–262.
3. Buss F, Kent H, Stewart M, Bailer SM, Hanover JA. Role of different domains in the self-association of rat nucleoporin p62. J Cell Sci 1994;107:631–638.
4. Melcak I, Hoelz A, Blobel G. Structure of Nup58/45 suggests flexible nuclear pore diameter by intermolecular sliding. Science 2007;315:1729–1732.
5. Schrader N, Stelter P, Flemming D, Kunze R, Hurt E, Vetter IR. Structural basis of the nic96 subcomplex organization in the nuclear pore channel. Mol Cell 2008;29:46–55.
6. Frey S, Gorlich D. A saturated FG-repeat hydrogel can reproduce the permeability properties of nuclear pore complexes. Cell 2007;130:512–523.
7. Van Impe K, Hubert T, De Corte V, Vanloo B, Boucherie C, Vandekerckhove J, Gettemans J. A new role for nuclear transport factor 2 and Ran: nuclear import of CapG. Traffic 2008;9:695–707.
8. Paschal BM, Gerace L. Identification of NTF2, a cytosolic factor for nuclear import that interacts with nuclear pore complex protein p62. J Cell Biol 1995;129:925–937.
9. Clarkson WD, Kent HM, Stewart M. Separate binding sites on nuclear transport factor 2 (NTF2) for GDP-Ran and the phenylalanine-rich repeat regions of nucleoporins p62 and Nsp1p. J Mol Biol 1996;263:517–524.
10. Bayliss R, Leung SW, Baker RP, Quimby BB, Corbett AH, Stewart M. Structural basis for the interaction between NTF2 and nucleoporin FxFG repeats. EMBO J 2002;21:2843–2853.
11. Bayliss R, Ribbeck K, Akin D, Kent HM, Feldherr CM, Gorlich D, Stewart M. Interaction between NTF2 and xFxFG-containing nucleoporins is required to mediate nuclear import of RanGDP. J Mol Biol 1999;293:579–593.
12. Rabut G, Doye V, Ellenberg J. Mapping the dynamic organization of the nuclear pore complex inside single living cells. Nat Cell Biol 2004;6:1114–1121.
13. Dultz E, Zanin E, Wurzenberger C, Braun M, Rabut G, Sironi L, Ellenberg J. Systematic kinetic analysis of mitotic dis- and reassembly of the nuclear pore in living cells. J Cell Biol 2008;180:857–865.
14. Joseph J, Dasso M. The nucleoporin Nup358 associates with and regulates interphase microtubules. FEBS Lett 2008;582:190–196.
15. Cho KI, Cai Y, Yi H, Yeh A, Aslanukov A, Ferreira PA. Association of the kinesin-binding domain of RanBP2 to KIF5B and KIF5C determines mitochondria localization and function. Traffic 2007;8:1722–1735.
16. Kasper LH, Brindle PK, Schnabel CA, Pritchard CE, Cleary ML, van Deursen JM. CREB binding protein interacts with nucleoporin-specific FG repeats that activate transcription and mediate NUP98-HOXA9 oncogenicity. Mol Cell Biol 1999;19:764–776.
17. Wang GG, Cai L, Pasillas MP, Kamps MP. NUP98-NSD1 links H3K36 methylation to Hox-A gene activation and leukaemogenesis. Nat Cell Biol 2007;9:804–812.
18. Palancade B, Liu X, Garcia-Rubio M, Aguilera A, Zhao X, Doye V. Nucleoporins prevent DNA damage accumulation by modulating Ulp1-dependent sumoylation processes. Mol Biol Cell 2007;18:2912–2923.
19. Joseph J, Liu ST, Jablonski SA, Yen TJ, Dasso M. The RanGAP1-RanBP2 complex is essential for microtubule-kinetochore interactions in vivo. Curr Biol 2004;14:611–617.
20. Zuccolo M, Alves A, Galy V, Bolhy S, Formstecher E, Racine V, Sibarita JB, Fukagawa T, Shiekhattar R, Yen T, Doye V. The human Nup107–160 nuclear pore subcomplex contributes to proper kinetochore functions. EMBO J 2007;26:1853–1864.
21. Dawlaty MM, Malureanu L, Jeganathan KB, Kao E, Sustmann C, Tahk S, Shuai K, Grosschedl R, van Deursen JM. Resolution of sister centromeres requires RanBP2-mediated SUMOylation of topoisomerase IIalpha. Cell 2008;133:103–115.
22. Blower MD, Nachury M, Heald R, Weis K. A Rae1-containing ribonucleoprotein complex is required for mitotic spindle assembly. Cell 2005;121:223–234.
23. Orjalo AV, Arnaoutov A, Shen Z, Boyarchuk Y, Zeitlin SG, Fontoura B, Briggs S, Dasso M, Forbes DJ. The Nup107–160 nucleoporin complex is required for correct bipolar spindle assembly. Mol Biol Cell 2006;17:3806–3818.
24. Jeganathan KB, Malureanu L, van Deursen JM. The Rae1-Nup98 complex prevents aneuploidy by inhibiting securin degradation. Nature 2005;438:1036–1039.
25. Lee SH, Sterling H, Burlingame A, McCormick F. Tpr directly binds to Mad1 and Mad2 and is important for the Mad1-Mad2-mediated mitotic spindle checkpoint. Genes Dev 2008;22:2926–2931.
26. Taddei A, Van Houwe G, Hediger F, Kalck V, Cubizolles F, Schober H, Gasser SM. Nuclear pore association confers optimal expression levels for an inducible yeast gene. Nature 2006;441:774–778.
27. Kirsh O, Seeler JS, Pichler A, Gast A, Muller S, Miska E, Mathieu M, Harel-Bellan A, Kouzarides T, Melchior F, Dejean A. The SUMO E3 ligase RanBP2 promotes modification of the HDAC4 deacetylase. EMBO J 2002;21:2682–2691.

28. Nagai S, Dubrana K, Tsai-Pflugfelder M, Davidson MB, Roberts TM, Brown GW, Varela E, Hediger F, Gasser SM, Krogan NJ. Functional targeting of DNA damage to a nuclear pore-associated SUMO-dependent ubiquitin ligase. Science 2008;322:597–602.
29. Rittmeyer EN, Daniel S, Hsu SC, Osman MA. A dual role for IQGAP1 in regulating exocytosis. J Cell Sci 2008;121:391–403.
30. Sakurai-Yageta M, Recchi C, Le Dez G, Sibarita JB, Daviet L, Camonis J, Souza-Schorey C, Chavrier P. The interaction of IQGAP1 with the exocyst complex is required for tumor cell invasion downstream of Cdc42 and RhoA. J Cell Biol 2008;181:985–998.
31. Inoue M, Chang L, Hwang J, Chiang SH, Saltiel AR. The exocyst complex is required for targeting of Glut4 to the plasma membrane by insulin. Nature 2003;422:629–633.
32. Grindstaff KK, Yeaman C, Anandasabapathy N, Hsu SC, Rodriguez-Boulan E, Scheller RH, Nelson WJ. Sec6/8 complex is recruited to cell-cell contacts and specifies transport vesicle delivery to the basal-lateral membrane in epithelial cells. Cell 1998;93:731–740.
33. Kawato M, Shirakawa R, Kondo H, Higashi T, Ikeda T, Okawa K, Fukai S, Nureki O, Kita T, Horiuchi H. Regulation of platelet dense granule secretion by the Ral GTPase-exocyst pathway. J Biol Chem 2008;283:166–174.
34. Hsu SC, Ting AE, Hazuka CD, Davanger S, Kenny JW, Kee Y, Scheller RH. The mammalian brain rsec6/8 complex. Neuron 1996;17:1209–1219.
35. Rosse C, Hatzoglou A, Parrini MC, White MA, Chavrier P, Camonis J. RalB mobilizes the exocyst to drive cell migration. Mol Cell Biol 2006;26:727–734.
36. Gromley A, Yeaman C, Rosa J, Redick S, Chen CT, Mirabelle S, Guha M, Sillibourne J, Doxsey SJ. Centriolin anchoring of exocyst and SNARE complexes at the midbody is required for secretory-vesicle-mediated abscission. Cell 2005;123:75–87.
37. Boyd C, Hughes T, Pypaert M, Novick P. Vesicles carry most exocyst subunits to exocytic sites marked by the remaining two subunits, Sec3p and Exo70p. J Cell Biol 2004;167:889–901.
38. He B, Xi F, Zhang X, Zhang J, Guo W. Exo70 interacts with phospholipids and mediates the targeting of the exocyst to the plasma membrane. EMBO J 2007;26:4053–4065.
39. Moore BA, Robinson HH, Xu Z. The crystal structure of mouse Exo70 reveals unique features of the mammalian exocyst. J Mol Biol 2007;371:410–421.
40. Munson M, Novick P. The exocyst defrocked, a framework of rods revealed. Nat Struct Mol Biol 2006;13:577–581.
41. Zuo X, Zhang J, Zhang Y, Hsu SC, Zhou D, Guo W. Exo70 interacts with the Arp2/3 complex and regulates cell migration. Nat Cell Biol 2006;8:1383–1388.
42. Pommereit D, Wouters FS. An NGF-induced Exo70-TC10 complex locally antagonises Cdc42-mediated activation of N-WASP to modulate neurite outgrowth. J Cell Sci 2007;120:2694–2705.
43. Caswell PT, Norman JC. Integrin trafficking and the control of cell migration. Traffic 2006;7:14–21.
44. Tayeb MA, Skalski M, Cha MC, Kean MJ, Scaife M, Coppolino MG. Inhibition of SNARE-mediated membrane traffic impairs cell migration. Exp Cell Res 2005;305:63–73.
45. Ward JJ, Sodhi JS, McGuffin LJ, Buxton BF, Jones DT. Prediction and functional analysis of native disorder in proteins from the three kingdoms of life. J Mol Biol 2004;337:635–645.
46. Liu J, Zuo X, Yue P, Guo W. Phosphatidylinositol 4,5-bisphosphate mediates the targeting of the exocyst to the plasma membrane for exocytosis in mammalian cells. Mol Biol Cell 2007;18:4483–4492.
47. Yeaman C, Grindstaff KK, Wright JR, Nelson WJ. Sec6/8 complexes on trans-Golgi network and plasma membrane regulate late stages of exocytosis in mammalian cells. J Cell Biol 2001;155:593–604.
48. Prigent M, Dubois T, Raposo G, Derrien V, Tenza D, Rosse C, Camonis J, Chavrier P. ARF6 controls post-endocytic recycling through its downstream exocyst complex effector. J Cell Biol 2003;163:1111–1121.
49. Oztan A, Silvis M, Weisz OA, Bradbury NA, Hsu SC, Goldenring JR, Yeaman C, Apodaca G. Exocyst requirement for endocytic traffic directed toward the apical and basolateral poles of polarized MDCK cells. Mol Biol Cell 2007;18:3978–3992.
50. Brown FD, Rozelle AL, Yin HL, Balla T, Donaldson JG. Phosphatidylinositol 4,5-bisphosphate and Arf6-regulated membrane traffic. J Cell Biol 2001;154:1007–1017.
51. Kawase K, Nakamura T, Takaya A, Aoki K, Namikawa K, Kiyama H, Inagaki S, Takemoto H, Saltiel AR, Matsuda M. GTP hydrolysis by the Rho family GTPase TC10 promotes exocytic vesicle fusion. Dev Cell 2006;11:411–421.
52. Stewart M. Molecular mechanism of the nuclear protein import cycle. Nat Rev Mol Cell Biol 2007;8:195–208.
53. Schwarz-Herion K, Maco B, Sauder U, Fahrenkrog B. Domain topology of the p62 complex within the 3-D architecture of the nuclear pore complex. J Mol Biol 2007;370:796–806.
54. Bernad R, van der Velde H, Fornerod M, Pickersgill H. Nup358/RanBP2 attaches to the nuclear pore complex via association with Nup88 and Nup214/CAN and plays a supporting role in CRM1-mediated nuclear protein export. Mol Cell Biol 2004;24:2373–2384.
55. Loiodice I, Alves A, Rabut G, Van OM, Ellenberg J, Sibarita JB, Doye V. The entire Nup107–160 complex, including three new members, is targeted as one entity to kinetochores in mitosis. Mol Biol Cell 2004;15:3333–3344.
56. Kalverda B, Fornerod M. The nuclear life of nucleoporins. Dev Cell 2007;13:164–165.
57. Matunis MJ, Pickart CM. Beginning at the end with SUMO. Nat Struct Mol Biol 2005;12:565–566.
58. Palancade B, Doye V. Sumoylating and desumoylating enzymes at nuclear pores: underpinning their unexpected duties? Trends Cell Biol 2008;18:174–183.
59. De Corte V, Bruyneel E, Boucherie C, Mareel M, Vandekerckhove J, Gettemans J. Gelsolin-induced epithelial cell invasion is dependent on Ras-Rac signaling. EMBO J 2002;21:6781–6790.
60. Zimmermann P, Meerschaert K, Reekmans G, Leenaerts I, Small JV, Vandekerckhove J, David G, Gettemans J. PIP(2)-PDZ domain binding controls the association of syntenin with the plasma membrane. Mol Cell 2002;9:1215–1225.
61. Bradford MM. A rapid and sensitive method for the quantitation of microgram quantities of protein utilizing the principle of protein-dye binding. Anal Biochem 1976;72:248–254.
62. Towbin H, Staehelin T, Gordon J. Electrophoretic transfer of proteins from polyacrylamide gels to nitrocellulose sheets: procedure and some applications. 1979. Biotechnology 1992;24:145–149.